Proceedings of the
Annual Stability Conference
Structural Stability Research Council
Baltimore, Maryland, April 10-13, 2018

Warping and Deformations in Profiled Steel Deck under Shear

Astrid W. Fischer[1], Guanbo Bian[2], Benjamin W. Schafer[3]

Abstract

The objective of this paper is to evaluate currently available methods for predicting the warping and other deformations that occur in bare steel deck profiles under shear. Profiled steel panels often serve as the diaphragm in single-story buildings and thus are the main element for distributing lateral forces to the walls. As a diaphragm they largely undergo in-plane shear. Thus, the in-plane shear stiffness of these panels is of crucial importance in design. The American Iron and Steel Institute (AISI) S310 Specification and Steel Deck Institute's Diaphragm Design Manual (DDM) provide an analytical approximation for determining the shear stiffness based on contributions from the deck in pure shear, connection slip, and warping of the deck. Due to the thin-walled nature of the deck geometric nonlinear deformations can be important and stability of the deck profile can also influence the stiffness results. The prediction of the warping deformations is based on a simplified two-dimensional beam on elastic foundation approximation that is explained in detail herein. This model is an approximation of the actual three-dimensional deformations. Shell finite element models are constructed in ABAQUS to examine the deck shear displacements and idealized boundary conditions are introduced to isolate the deck deformations and compare with the approximations in DDM/AISI S310. Comparison of the results indicates that improvements in the DDM/AISI S310 model for predicting warping are possible; as is generalization of the approximate method employed. Shell finite element predictions of pure shear stiffness and connection slip are found to be in good agreement with DDM/AISI S310. This work is part of the larger Steel Diaphragm Innovation Initiative and aims to understand and optimize the behavior of steel deck diaphragms.

[1] Ph.D. Student, Civil Engineering, Johns Hopkins University, winther@jhu.edu
[2] Financial Engineer, Fannie Mae, formerly at Johns Hopkins University, bian@jhu.edu
[3] Professor, Civil Engineering, Johns Hopkins University, schafer@jhu.edu

1. Introduction

Profiled steel panels, i.e., steel deck, are roll-formed from thin steel sheets and can result in simple corrugated shapes or relatively complex longitudinal profiles with additional transverse features such as embossments. The corrugation layout studied in this paper is constrained to the configuration illustrated in Figure 1. Dimensions of four typical diaphragms studied herein are listed in Table 1. Profiled steel panels are often used as the walls and roofs in many metal buildings. In addition to distributing out-of-plane loads to the structure they often serve as the diaphragm in buildings and thus are the main element for distributing lateral forces to the walls, and largely act as an in-plane shear panel.

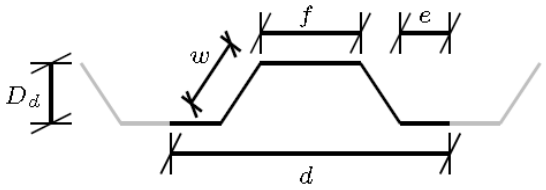

Figure 1: Nomenclature for typical profiled steel panel corrugation

Table 1: Typical dimensions of profiled steel panels

ID[1]		D_d	w	d	$2e$	f	s[2]
WR	$[in]$	1.47	1.53	6.00	1.56	3.56	8.19
	$[mm]$	*37.34*	*38.86*	*152.40*	*39.62*	*90.42*	*208.03*
IR	$[in]$	1.47	1.59	6.00	0.53	4.24	7.95
	$[mm]$	*37.34*	*40.39*	*152.40*	*13.46*	*107.70*	*201.93*
NR	$[in]$	1.47	1.51	6.00	0.36	4.99	8.36
	$[mm]$	*37.34*	*38.35*	*152.40*	*9.14*	*126.75*	*212.34*
DR	$[in]$	3.00	3.07	8.00	1.49	5.24	12.86
	$[mm]$	*76.20*	*77.98*	*203.20*	*37.85*	*133.10*	*326.64*

1. ID: wide rib (WR), intermediate rib (IR), narrow rib (NR) and deep rib (DR)
2. Perimeter length of profile $s=2e+2w+f$

The shear behavior of the diaphragm is important in design. The American Iron and Steel Institute (AISI) S310 Specification (AISI, 2013) and the Steel Deck Institute's (SDI's) Diaphragm Design Manual (DDM) (Luttrell, 2015) provide an analytical approximation for determining the bare diaphragm's strength and shear stiffness, where the strength is based on the lesser of the strength of the connections and buckling capacity of the steel plate, and the stiffness is based on contributions from the deck in pure shear, connection slip, and deck warping. This paper focuses primarily on the stiffness of the diaphragm. In particular, the warping contribution to the in-plane deck flexibility in shear, as given in AISI S310 and DDM, is based on a simplified two-dimensional beam on elastic foundation approximation. Expressions for the spring stiffness of the elastic foundation approximation are only provided for steel diaphragms with corrugation layout equal to the one in Figure 1. However, it is possible to calculate similar spring constants through a beam finite element (FE) model, where the complexity of the corrugation layout does not hinder the designer in finding the additional flexibility of the diaphragm due to deck warping displacements – this idea is studied herein.

2. AISI S310/DDM Calculations for Shear Stiffness

Corrugations in the diaphragm cause reductions in the in-plane shear stiffness below that of an equivalent flat plate, and the estimate for the reduced shear stiffness is essential for design. The deformations in a shear loaded diaphragm are assumed to be composed of deformations from pure shear, fastener slip at connections, and lastly, warping displacements of the deck profile, which will occur for diaphragms with free ends. (Luttrell & Huang, 1981)

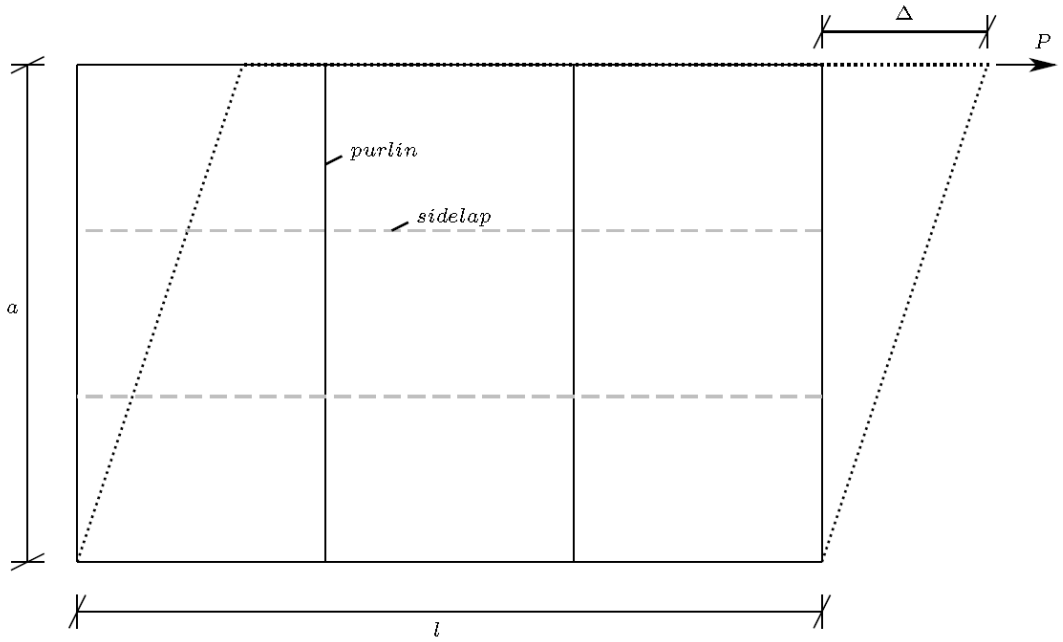

Figure 2: Diaphragm subjected to shear load and shear deformation.

Consider the diaphragm in Figure 2 subjected to pure shear approximated as a flat plate with thickness t, length l and depth a, under a shear force P and deflecting Δ, then the shear stiffness (G') may be written as:

$$G' = Gt = \frac{P/lt}{\Delta/a}t = \frac{Pa}{l\ \Delta} = \frac{Pa}{l\left(\Delta_s + \Delta_f + \Delta_w\right)} \tag{1}$$

where Δ_s, Δ_f, and Δ_w are the components of Δ associated with pure shear, slip of the fasteners, and warping deformations. The diaphragm stiffness, as in AISI S310, may alternatively be expressed in terms of a slip coefficient C and a warping coefficient D_n:

$$G' = \frac{E\ t}{2(1+\nu)\frac{s}{d} + C + D_n} \tag{2}$$

where E, is the modulus of elasticity, ν, is the Poisson's ratio, and s/d is the ratio of the profile perimeter length to the flat plate length, provided in Table 1 for selected profiles.

2.1 Shear Strain Deformations

For pure shear the shear stress is assumed to be constant throughout, which will result in a shear deformation from the shear stress of:

$$\Delta_s = \frac{Pa}{G\ l\ t}\frac{s}{d} \tag{3}$$

where s/d corrects for the longer path that the shear acts over due to the corrugations.

2.2 Fastener Slip

The deformation associated with fastener slip (i.e., localized deformations at connectors largely due to bending and bearing displacement localized in the thin steel sheet) is found by imposing a deformation of δ_f on the edge of a single panel, and assuming each fastener will displace an amount depending on the distance from the centerline, and each fastener will contribute with a force, which is a function of the flexibility of the fastener connection. See AISI S310/DDM 04 for a free body diagram of this equilibrium state. The forces from each fastener are summed, and the force the single panel can resist when displaced δ_f at top and bottom is:

$$\delta_f = S_f P \frac{1}{2\ \alpha_e + n_p \alpha_p + 2\ n_s \alpha_s{}'} \tag{4}$$

where S_f is the flexibility of a structural fastener/connection, α_e and α_p are the sum of distances from centerline to fastener location on an edge member or a purlin; $\alpha_s' = S_f/S_s$ and is the structural to sidelap fastener flexibility ratio and n_p and n_s are the number of purlins in the diaphragm and the number of sidelap fasteners. The total shear deformation from fastener slip from multiple panels then becomes:

$$\Delta_f = 2\delta_f\ n_d = \ S_f P \frac{2\ n_d}{2\ \alpha_e + n_p \alpha_p + 2\ n_s \alpha_s{}'} \tag{5}$$

Where n_d is the number of panels along the height of the diaphragm: $n_d = a/w_d$, where w_d is the width of a panel. Rearranging we may also express this as the slip coefficient:

$$C = \frac{Etl}{Pa}\Delta_f = \frac{E\ t\ l}{w_d}\ S_f \frac{2}{2\ \alpha_e + n_p \alpha_p + 2\ n_s \alpha_s{}'} \tag{6}$$

2.3 Warping Deformations

The last contribution to the shear flexibility comes from the warping deformations of the diaphragm when subjected to shear loads. Considering a single corrugation (flute) with a load *P* along each side of the flute, the top flange will displace perpendicular to the direction of loading, see Figure 3a.

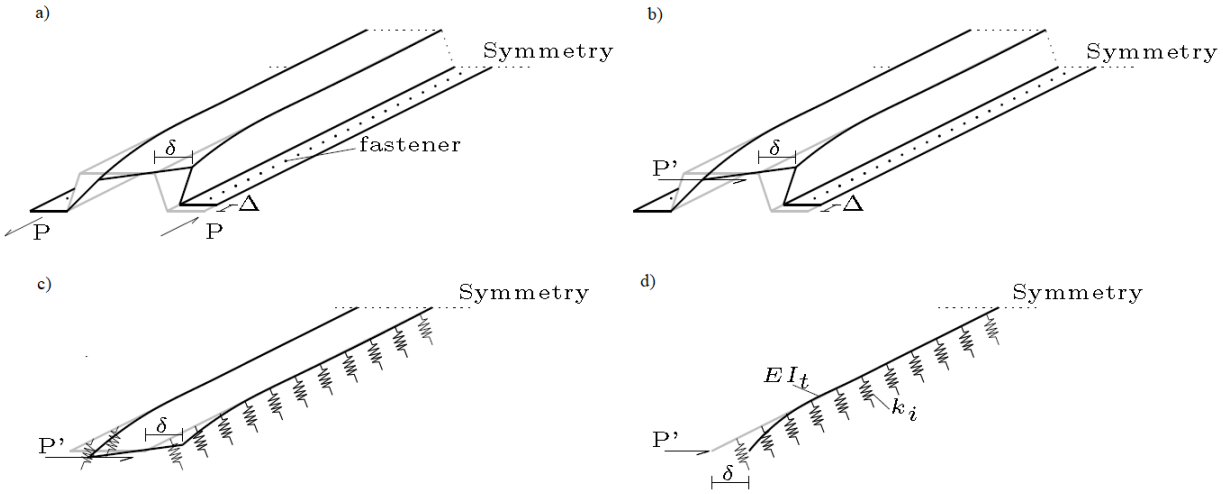

Figure 3: Warping displacements of a single corrugation due to shear loads along the length.

Introducing a load P' acting on the top flange at both ends is now causing this deformation, see Figure 3b. To estimate the warping displacement, a beam on elastic foundation is used to approximate the deformations of the top flange, see Figure 3c. The top flange is the beam and the webs are considered to be foundation springs connecting the flange to the fasteners, see Figure 3d. The stiffness of the corrugation is first estimated for use as the spring stiffness in the beam on elastic foundation approximation.

2.3.1 Spring constant

The method used in (Luttrell & Huang, 1981) and AISI S310 to find the spring constants is first to find the flexibilities of a single corrugation with simple supports. Three flexibilities are found from two different load cases of the single corrugation: A horizontal unit load applied at the top flange, and a horizontal unit load at the bottom flange. The displacements at the top and bottom flange equal the flexibilities (two of the flexibilities are equal: $\xi_{12} = \xi_{21}$). The flexibilities are then used to calculate the displacements at the upper and lower flanges of one or more corrugations and the displacements are directly related to the spring constants:

$$k_i = \frac{P_i}{\delta_i} \tag{7}$$

Where P_i is the applied load at the location of the displacement δ_i. The flexibilities and spring constants can be found in Appendix to this paper and in AISI S310 Appendix 1 Eq. (1.4-8)-(1.4-20).

Some simplifications were introduced in the approximation to determine the spring constant for a single or multiple corrugations between fasteners. For one, the models employ hinges at the bottom flanges, for all corrugation layouts. Moreover, for multiple corrugations between fasteners, the lower flanges are supported by simple pin connections with horizontal rollers. To some extend this pin support with rollers can be justified by the presence of purlins, which provide supports for the corrugation.

2.3.2 Beam on Elastic Foundation

The warping displacement in Figure 3, can be expressed as a beam (top flange/flute) supported by an elastic foundation along its entire length, as introduced by (Luttrell & Huang, 1981). The diaphragm flute is symmetric as is the loading, therefore only half of the flute is considered in the expression for the displacement. The resulting beam on elastic foundation is illustrated in Figure 4.

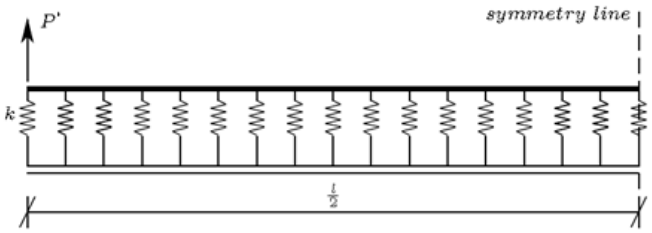

Figure 4: Beam (top flange) on elastic foundation (corrugation and supports) model for warping.

The governing differential equation and trial solution for this model is:

$$EI\, y^{iv} + ky = 0 \tag{8a}$$

$$\begin{aligned} y = {} & A\cosh(\beta_i x)\cos(\beta_i x) + B\sinh(\beta_i x)\cos(\beta_i x) \\ & + C\cosh(\beta_i x)\sin(\beta_i x) + D\sinh(\beta_i x)\sin(\beta_i x) \end{aligned} \tag{8b}$$

where $\beta_{t1}^4 = \frac{k_{t1}}{4EI_t}$ is a stiffness parameter for a single top flange, note that different fastener layout will provide different spring stiffnesses, and therefore also different stiffness parameters β_i. I_t is the moment of inertia of the top flange and $1/6$ of the top part of the web (empirically determined).

$$I_t = \frac{tf^2}{12}(f + w) \tag{9a}$$

$$I_b = \frac{te^2}{3}(2e + w) \tag{9b}$$

The beam in Figure 4 has boundary conditions of: $y(l/2) = 0,\ y''(l/2) = 0,\ y''(0) = 0,\ y'''(0) = P'/EI_t$, where $P' = P\,f/l$ is the force acting at the edge of the flange. Applying the boundary conditions to the solution in Eq. 8b results in a deflection at the free end equal to:

$$\delta_{t1} = y(0) = \frac{P'}{2\beta_{t1}^2\, EI_t}\, A_{t1} = 2P'\frac{\beta_{t1}}{k_{t1}}\, A_{t1} \tag{10a}$$

$$A_i = \frac{\sinh\left(\frac{\beta_i l}{2}\right)^2 + \sin\left(\frac{\beta_i l}{2}\right)^2}{\sinh\left(\frac{\beta_i l}{2}\right)\cosh\left(\frac{\beta_i l}{2}\right) - \cos\left(\frac{\beta_i l}{2}\right)\sin\left(\frac{\beta_i l}{2}\right)} \tag{10b}$$

2.3.3 Warping Coefficient

The warping displacement can be expressed as a warping constant, which is used in DDM and AISI S310. Converting the displacement to the constant is done in several steps. First the corresponding shear displacement along the length of the flute is found, followed by summation of the individual flange's contribution to the total displacement between fasteners:

$$\delta_{dn} = \sum_n \delta_{ti} \frac{f}{l} + \delta_{bi} \frac{2e}{l} \tag{11}$$

The warping displacement is the ratio of total height of the diaphragm to the distance between fasteners:

$$\Delta_w = \frac{a}{nd} \delta_{dn} = \frac{2P}{nd} \frac{f^2}{l^2} \sum_n \frac{\beta_{ti}}{k_{ti}} A_{ti} + \left(\frac{2e}{f}\right)^2 \frac{\beta_{bi}}{k_{bi}} A_{bi} \tag{12}$$

Lastly, we come to the warping coefficient D_n:

$$D_n = \frac{Etl}{Pa} \Delta_w = \frac{2Et}{nd} \frac{f^2}{l} \sum_n \frac{\beta_{ti}}{k_{ti}} A_{ti} + \left(\frac{2e}{f}\right)^2 \frac{\beta_{bi}}{k_{bi}} A_{bi} \tag{13}$$

AISI S310 assumes $A_i = 1$ and it is therefore omitted in the expression for the warping coefficient in the Specification. If A_i is omitted from the expression $D = D_n L$ is a constant, and is listed in Table 3.3-2 in DDM and Table C-1.2 in the commentary to Appendix 1 in AISI S310.

2.4 Intermediate Purlin Support

Diaphragm panels supported by intermediate purlins will have a smaller reduction of the shear stiffness associated with warping. The purlins ensure the diaphragm panels are "pinned" to a location, and thus not free to warp unconstrained along the entire panel, this increases the force needed to warp the panel. The purlin effectiveness factor was first presented by (Bryan & El-Dakhakhni, 1968) and later in (Luttrell & Huang, 1981). The idea is that the panel with intermediate purlin supports can be presented by several smaller panels with no intermediate purlins, see Figure 5.

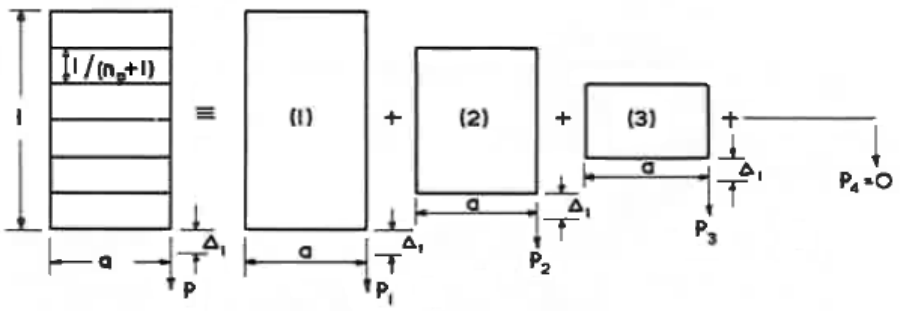

Figure 5: Panel with intermediate purlins and smaller panels with no intermediate purlins.
From (Bryan & El-Dakhakhni, 1968)

Each of the panels with no intermediate purlins is assumed to deform Δ_{dn} caused by the forces P_1, P_2, $P_3 \ldots P_n$, applied at each panel. The strain energy in the panels associated with the applied load and deformation is dependent on the length of the panel:

$$U_i = \frac{P_i^2}{\left(l - \frac{2(i-1)}{n_p+1}\, l\right)^2}\, C \tag{14}$$

Differentiating the panels' strain energies with the load P_i results in the same constant for all the panels, this relation can be used to express the loads P_2,$P_3 \ldots P_n$ in terms of P_1:

$$P_i = \left(1 - \frac{2\,(i-1)}{n_p+1}\right)^2 P_1 \tag{15}$$

Finally, the load P on the panel with intermediate purlin supports, are the sum of the loads acting on the sub panels:

$$P = P_1 + P_2 + P_3 + .. + P_n = \sum_{i=1}^{n} \left(1 - \frac{2(i-1)}{n_p+1}\right)^2 P_1 = \frac{1}{\rho}\, P_1 \tag{16}$$

Determining the constant ρ for different n_p, results in the values in Table 1.3-1 in AISI and Table 3.3-3 in DDM04.

3. 2D FE Models for Warping Calculation

Simple linear elastic FE beam models can replace the beam on elastic foundation calculations used in AISI S310 and DDM (i.e., Appendix and Eq. 8-11) for finding the warping displacement of the diaphragm. This potentially provides a more general approach for handling alternative panel profiles and engineers may more readily follow the beam analysis as opposed to the differential equations used in the current solution. The software Mastan2 version 3.4 is used to replace the AISI S310 expressions.

3.1 Foundation Spring Stiffness

Rather than employing the hand solutions introduced in Section 2.3.1/Appendix one may find the spring constants that support warping of the flange directly from a beam FE model. The corrugations between two fasteners are modeled as beam elements, apply a unit load at the top of each flute, and in the case of bottom flutes apply a load of size $a' = 2e/f$ at each bottom flute. Pin supports are applied at the ends, and hinges and simple support with rollers are applied at each bottom flute, see Figure 6 for an example.

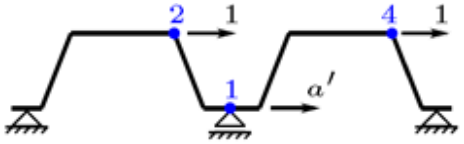

Figure 6: FE model of corrugations presenting alternate fastener layout.

Linear elastic analysis is executed on the model, and the horizontal displacements at each location of the applied loads are extracted. The spring constant is then the load divided by the associated displacement:

$$k_i = \frac{P_i}{\delta_i} \tag{17}$$

There can be multiple spring constants from the one model, depending on the number of corrugations. A single corrugation with fasteners at each bottom flute, has a single spring stiffness for the top flange, two corrugations will have a spring constant for the bottom flute and one for each of the top flutes, which will be equal due to symmetry.

Table 2 lists the spring constants for the wide rib (WR) diaphragm type with fastener layout in each alternate corrugation using the method introduced in Section 2.3.1/Appendix and by using the FE model described here. Since the two approaches employ the same mechanical assumptions they are essentially coincident. This remains true for other diaphragm types (see dimensions listed in Table 1) and fastener spacing up to four corrugations between fasteners as provided in Appendix Table 4.

Table 2: Spring constant for alternative fastener layout. The constants are found by use of linear elastic FE models and the expressions in AISI S310 Appendix 1.

			AISI S310		FEM		Difference - %	
	t		k_{t2}	k_{b2}	k_{t2}	k_{b2}	k_{t2}	k_{b2}
WR	0.0295 in	[psi]	15.98	3.89	15.93	3.88	0.30	0.21
	0.7493 mm	*[ksi]*	110.18	26.79	109.85	26.74		
	0.0358 in	[psi]	28.56	6.95	28.47	6.93	0.30	0.21
	0.9093 mm	*[ksi]*	196.92	47.88	196.33	47.78		
	0.0474 in	[psi]	66.29	16.12	66.09	16.09	0.31	0.21
	1.2040 mm	*[ksi]*	457.06	111.14	455.64	110.91		
	0.0598 in	[psi]	133.11	32.37	132.68	32.30	0.32	0.22
	1.5189 mm	*[ksi]*	917.78	223.18	914.82	222.69		

3.2 Beam on Elastic Foundation

The AISI S310/DDM beam on elastic foundation expression can also be replaced with a simple FE model of a beam connected to a foundation of truss element "springs". As the number of truss element springs is increased the response converges to the classical beam on elastic foundation solution. A beam with bending stiffness EI_t (from Eq. 9a) of length l divided into $(n-1)$ elements and n nodes is subjected to vertical loads at its ends in opposite directions. The beam is continuous and is pin connected to vertical beam elements at each node (no moment transfer between the vertical support beams and the horizontal continuous beam). The axial stiffness of the vertical beam elements, i.e. the "truss" spring is:

$$EA = \frac{k\, L_b\, l}{n} \tag{18}$$

where L_b is the length of the vertical beam elements, k is the continuous spring stiffness of the elastic foundation, which here is the spring stiffness found in the section above or by Eq. A3b in the Appendix.

The FE results are sensitive to the number of elements, convergence of a typical model is provided in Figure 7. At 100 elements the difference with the analytical solution is 1.1%.

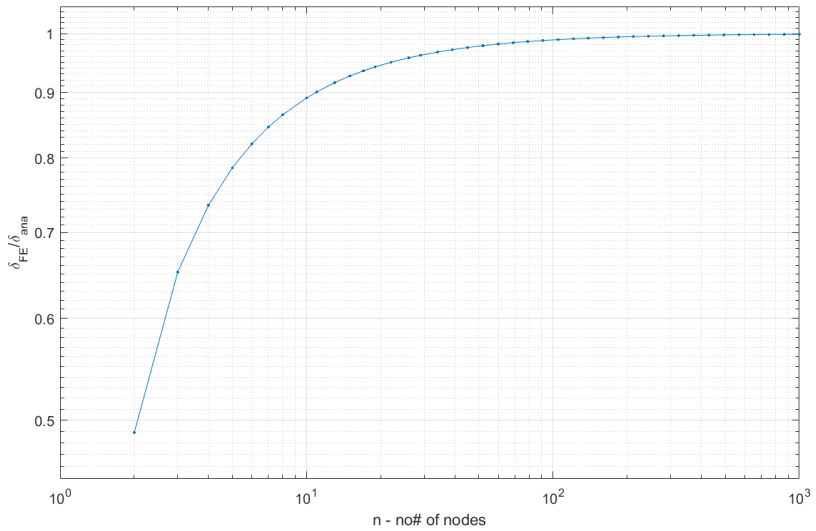

Figure 7: Convergence plot of the FE beam on elastic foundation displacement compared with the analytical solution.

This section shows that the general warping derivations of (Luttrell & Huang, 1981) as used today in AISI S310 or DDM may be understood as the result of the application of straightforward 2D beam element models. In fact, the warping deformation or warping coefficient may be arrived at directly from such simple models. This is a promising result as it makes generalization of the method to any unique profile much less cumbersome than re-deriving the complete expressions (see Appendix). A separate question remains, what is the accuracy of this approach. That aspect is explored in the following section.

4. 3D Models in Abaqus

A general examination of the performance of the AISI S310/DDM stiffness expressions was performed in (Bian & Schafer, 2017) and (Bian, et al., 2016). That work indicated that the AISI S310/DDM expressions for pure shear are consistent with 3D shell finite element models. The work also indicated that the influence of connection flexibility (slip) is reasonably captured by the AISI S310/DDM expressions. However, the previous work concluded that the existing AISI S310/DDM expressions for warping may require improvement. All previous modeling was conducted on full multi-panel diaphragms – similar to cantilever diaphragm tests, and it was concluded that a more fundamental treatment was needed.

A 3D shell finite element model was developed herein to explore and isolate the influence of warping deformations on panels. The models are built with shell elements of a single corrugation of the WR diaphragm type (see Table 1 for dimensions) with length l and thickness t. The

material is linear elastic steel with Young's modulus $E = 29500\ ksi\ (203395\ MPa)$ and poisson's ratio $\nu = 0.3$. A general static step is used with node (0,0,0) pinned in all three directions, and node $(l, 0,0)$ pinned in the y- and z-direction. The edges along the flute are pinned in the y-direction. Shear shell edge loads are applied on all edges of the model, with load $\tau' = 1000 kips/in$ with directions that represents a plate in pure shear. The element type used for the models is S8R5 this is a quadratic shell element with reduced integration and 5 DOF per node. The mesh size is chosen to be $e/6$ to ensure a fine mesh over the smaller parts of the flute.

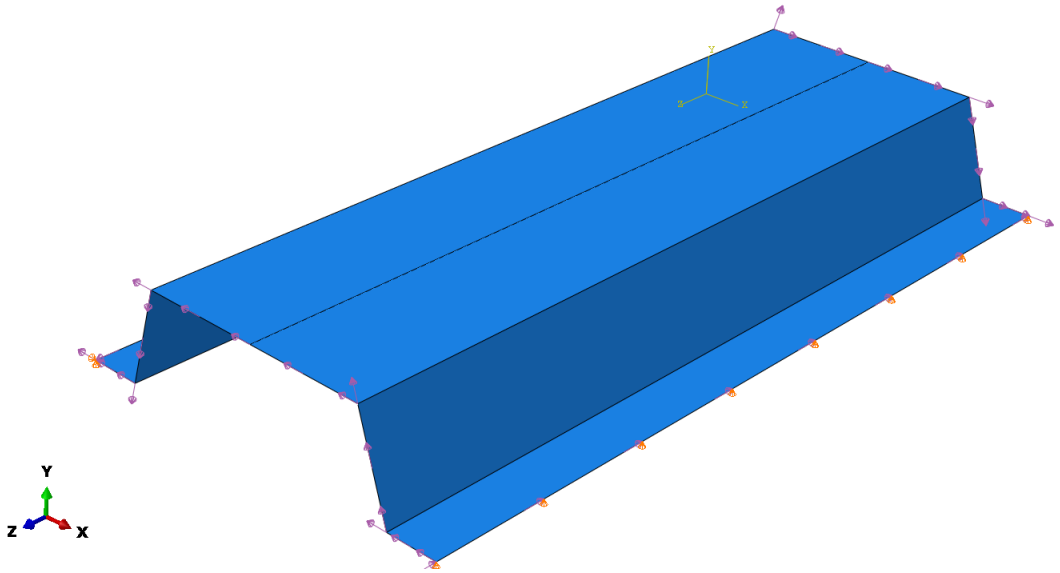

Figure 8: Abaqus model of single corrugation.

A simple linear elastic analysis is performed on the model and the maximum shear displacement is extracted. Since there are no fasteners and all member edges are loaded only the pure shear and warping contribute to the solution. The warping coefficient can be expressed in terms of the edge load and the shear displacement. Rewriting Eq. 1 and Eq. 2 with $\Delta_f = C = 0$ the warping coefficient may be expressed as:

$$D_n = \frac{E\ t\ l}{a}\frac{\Delta}{P} - 2\ (1+\nu)\frac{s}{d} \tag{19}$$

For lengths between 48 – 240 in. (i.e., 4 – 20 ft or 1.2-6.1 m) the warping coefficient D_n remains constant, see Table 3. This is not in agreement with AISI S310/DDM, where $D = D_n l$ is a constant and takes a value much larger than found with Abaqus. The results are provided in Table 4, differences are greater than observed in (Bian & Schafer, 2017), but follow the same trend – i.e. the shell models indicate significantly less warping deformation than the beam on elastic foundation solution.

Table 3: Warping coefficient D_n found with models in Abaqus and table values of the constant $D = D_n l$ from Table C-1.2 in AISI S310.

	t [in] *[mm]*	AISI S310 D table values [in] *[m]*	Abaqus models D_n $[10^{-3}]$
WR	0.0295 *0.75*	1237 *31.40*	3.850229
	0.0358 *0.91*	925 *23.50*	3.846935
	0.0474 *1.20*	607 *15.40*	3.845853
	0.0598 *1.52*	429 *10.90*	3.849885

The results of the model of the WR deck with t =0.0295 in (0.75 mm) are provide in Figure 9. The shear stress is essentially constant and matches the applied load and geometry: the associated calculated shear stress and the shear stress from the model equals $\tau = P/(l\,t) = 33.8983\ 10^3\ ksi$. However, the stresses at the free ends of the model are slightly elevated due to the additional warping deformation that occurs.

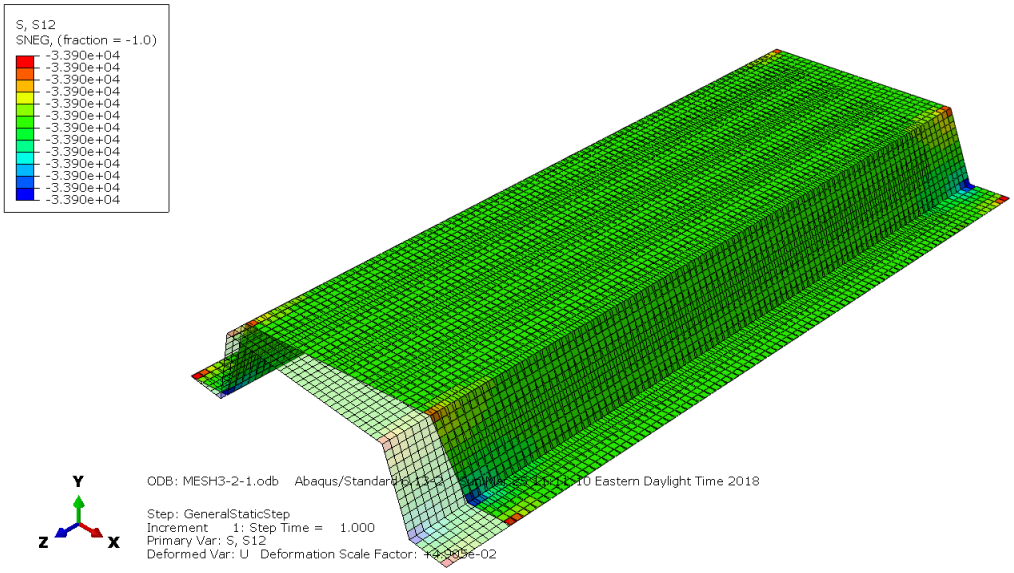

Figure 9: Deformed and undeformed Abaqus model of a single corrugation.

7. Discussion

The calculations in AISI S310 Appendix 1 to determine the warping coefficient D_n are laborious for even a simple deck corrugation. The calculations are straightforward, but assumptions behind the models, particularly in AISI S310, are not necessarily clear. If web or flange stiffeners are introduced to the cross-section, or another type of diaphragm corrugation is used, the current calculation procedure does not make it easy to determine this coefficient for warping.

For warping the AISI S310 calculations could be replaced by two simple beam finite element models – one to find the cross-section stiffness that helps to restrain warping and a second to apply that stiffness as a resisting foundation in approximating expected warping of the top flange. The methods are shown to be the same for a series of known cross-sections. The approach would be unchanged for more complex cross-sections and thus provides a simple analysis alternative to the current prescriptive expressions.

The 3D shell finite element model in ABAQUS predicts a stiffer response (less warping displacement) than the AISI S310/DDM method. Overall the AISI S310/DDM stiffness correlates reasonably with experiments (O'Brien, et al., 2017) suggesting that the approach is well founded. However, while the AISI S310/DDM warping model is mechanically inspired, it is not an accurate representation of the actual behavior. The foundation stiffness and the boundary conditions are very rough approximations of the actual condition. The selection of the top flange and tributary width of web is also empirical. The model includes some of the key mechanics associated with deck warping, but appears to not be an accurate representation of the actual 3D behavior. This is consistent with findings in (Bian & Schafer, 2017).

Future studies could consider different boundary conditions and loading cases in the shell FE models to potentially find warping displacements that agree more with the values giving in the Specification and to better understand what assumptions there were made in creating the warping coefficients. The most obvious next step in determining in necessary improvements is to use the more mechanically correct estimations of warping and compare them with the available test data, as summarized in (O'Brien, et al., 2017), and from this determine if the predicted deflections are improved. If yes, then changes may be warranted. If no, then it may need to be recognized that the current expressions approximate more than just warping deformations.

8. Conclusions

In this paper the current formulation used in design for determining the shear flexibility of profiled steel panels caused by warping displacement at the ends are investigated and new methods to find this flexibility presented. The formulas for warping flexibility in the American Iron and Steel Institute (AISI) S310 Specification are for one type of diaphragm corrugation, with no web or flange stiffeners and replication of the formulas for improved cross-sections are not supported. It is shown herein that the AISI S310 formulation for warping deformation is mechanically equivalent to a beam element model of the top flange (length equal to the deck span length) supported by springs which are developed from exercising an additional beam element model of the cross-section profile to find the spring stiffness. This model can readily be extended to other deck profiles. Additional studies were conducted to examine the validity of the AISI S310 warping predictions using ABAQUS shell finite element models. The shell models predict considerably less warping deformation than the AISI S310 approach. Additional study is needed to resolve this discrepancy and possible future research is discussed herein.

Acknowledgments

The authors gratefully acknowledge the financial support of the US National Science Foundation through grant CMMI-1562821 and of industry through the Steel Diaphragm Innovation Initiative (SDII). Collaborators in the SDII project have provided the authors with assistance throughout the work on this paper, and acknowledge the ideas and contributions they have given. Any

opinions, findings, and conclusions or recommendations expressed in this material are those of the authors and do not necessarily reflect the views of the National Science Foundation or other sponsors.

References

AISI, 2013. *North American Standard for the Design of Profiled Steel Diaphragm Panels.* s.l.:S310.

Bian, G. & Schafer, B. W., 2017. *Shell Finite Element Modeling of Elastic Shear Stiffness of Bare Steel Deck,* Baltimore, MD: Steel Diaphragm Innovation Initiative (SDII).

Bian, G., Torabian, S. & Schafer, B., 2016. *Reduced Order Models for Profiled Steel Diaphragm Panels.* Baltimore, CCFSS.

Bryan, E. R. & El-Dakhakhni, W. M., 1968. Shear Flexibility and Strength of Corrugated Decks. *Journal of the Structural Division, ASCE,* pp. pp. 2544-2580.

Luttrell, L., 2015. *Diaphragm Design Manual, edition 4,* s.l.: SDI.

Luttrell, L. D. & Huang, H.-T., 1981. *Steel Deck Diaphragm Studies,* Morgantown, West Virginia: The Steel Deck Institute.

O'Brien, P., Eatherton, M. & Easterling, W., 2017. *Characterizing the load-deformation behavior of steel deck diaphragms using past test data.* [Online]
Available at: https://jscholarship.library.jhu.edu/handle/1774.2/40633
[Accessed 24 03 2018].

Appendix

Spring Constants from AISI S310 Appendix 1

Three flexibility expressions for a single simple supported corrugation (also found in AISI S310 Appendix 1 Eq. (1.4-8)-(1.4-10)):

$$EI\,\xi_{11} = \frac{D_d^3}{3}\,(2w + 3f) \tag{A1a}$$

$$EI\,\xi_{22} = \frac{D_d^2}{12\,d^2}\left(s\,(4e^2 - 2ef + f^2) + d^2\,(3f + 2w)\right) \tag{A1b}$$

$$EI\,\xi_{12} = \frac{D_d^2}{6}(2w + 3f) = \frac{EI\xi_{11}}{2} \tag{A1c}$$

The spring constants are the stiffness of the webs supporting the flanges, using the flexibilities and the principle of superposition, the displacement of the corrugation can be determined. The fastener layout comes into play to set up the relations between forces and displacements. For fasteners between each corrugation, a single corrugation is considered, see Figure 10, where forces are applied at node 1 and 2, note that the right support is now a pin support without rollers, which gives a displacement $\Delta_1 = 0$:

$$\begin{bmatrix} 0 \\ \Delta_2 \end{bmatrix} = \begin{bmatrix} \xi_{11} & \xi_{12} \\ \xi_{12} & \xi_{22} \end{bmatrix} \begin{bmatrix} Q_1 \\ F \end{bmatrix} \tag{A2}$$

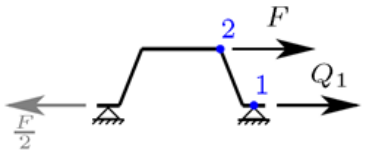

Figure 10: Single flute case, fastener between each corrugation, the forces and reactions are illustrated.

Solving these linear equations, the displacement and the corresponding spring stiffness can be found for a single corrugation:

$$\Delta_2 = -\frac{\xi_{12}^2}{\xi_{11}}\,F + \xi_{22}F \tag{A3a}$$

$$k_{t1} = \frac{F}{\Delta_2} = \frac{\xi_{11}}{\xi_{22}\xi_{11} - \xi_{12}^2} \tag{A3b}$$

For two flutes between fasteners, two corrugations are connected. A load F is applied at the two top flanges and a load $a'F$ at the bottom flange, see Figure 11, this load is divided evenly between the two corrugations, where $a' = 2e/f$ is the equivalent force multiplier for the lower flange:

$$\begin{bmatrix} \Delta_1 \\ \Delta_2 \end{bmatrix} = \begin{bmatrix} \xi_{11} & \xi_{12} \\ \xi_{12} & \xi_{22} \end{bmatrix} \begin{bmatrix} \frac{a'F}{2} \\ F \end{bmatrix} \tag{A4a}$$

$$\begin{bmatrix} \Delta_1 \\ \Delta_4 \end{bmatrix} = \begin{bmatrix} \xi_{11} & \xi_{12} \\ \xi_{12} & \xi_{22} \end{bmatrix} \begin{bmatrix} \frac{a'F}{2} \\ F \end{bmatrix} \tag{A4b}$$

$$k_{t2} = \frac{F}{\Delta_2} = \frac{1}{\xi_{22} + \frac{a'}{2}\xi_{12}} \tag{A5a}$$

$$k_{b2} = \frac{a'F}{\Delta_1} = \frac{a'}{\xi_{12} + \frac{a'}{2}\xi_{11}} \tag{A5b}$$

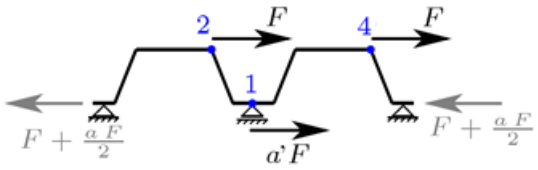

Figure 11: Double flute case, fastener between very other corrugations. The forces and reactions are illustrated.

Three flutes between fasteners, means three corrugations are connected and a load F is applied at the three top flanges and a load $a'F$ at the two bottom flanges. The middle corrugation is only subjected to a load at the top flange and reaction forces, additionally it also feels the deformation from the first corrugation. The first and last corrugations are the same, with the same loads.

$$\begin{bmatrix}\Delta_1\\ \Delta_2\end{bmatrix} = \begin{bmatrix}\xi_{11} & \xi_{12}\\ \xi_{12} & \xi_{22}\end{bmatrix}\begin{bmatrix}\frac{F}{2} + a'F\\ F\end{bmatrix} \tag{A6a}$$

$$\begin{bmatrix}\Delta_3\\ \Delta_4\end{bmatrix} = \begin{bmatrix}\xi_{11} & \xi_{12}\\ \xi_{12} & \xi_{22}\end{bmatrix}\begin{bmatrix}-\frac{F}{2}\\ F\end{bmatrix} + \Delta_1 \tag{A6b}$$

$$\begin{bmatrix}\Delta_3\\ \Delta_6\end{bmatrix} = \begin{bmatrix}\xi_{11} & \xi_{12}\\ \xi_{12} & \xi_{22}\end{bmatrix}\begin{bmatrix}\frac{F}{2} + a'F\\ F\end{bmatrix} \tag{A6c}$$

$$k_{t3} = \frac{F}{\Delta_2} = \frac{1}{\xi_{22} + \left(a' + \frac{1}{2}\right)\xi_{12}} \tag{A7a}$$

$$k_{b3} = \frac{a'F}{\Delta_1} = \frac{a'}{\xi_{12} + \left(a' + \frac{1}{2}\right)\xi_{11}} \tag{A7b}$$

$$k_{tc3} = \frac{a'F}{\Delta_4} = \frac{a'}{\frac{1}{2}\xi_{12} + \xi_{22} + \left(a' + \frac{1}{2}\right)\xi_{11}} \tag{A7c}$$

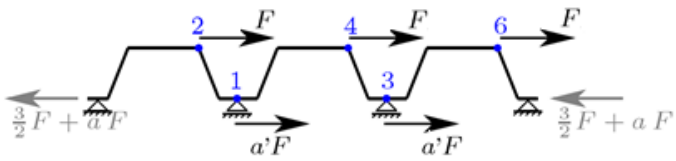

Figure 12: Triple flute case, fastener between very third corrugations. The forces and reactions are illustrated.

Same procedure can be applied on more flutes between fasteners.

Table 4: Comparison of spring stiffness results of the four diaphragm types listed in Table 1 and Figure 1. Comparison between expression provided in AISI S310 and linear elastic FE model of a single, double, and triple corrugation.

			AISI s310						FEM						Difference [%]					
	t		kt1	kt2	kt3	kb2	kb3	ktc3	kt1	kt2	kt3	kb2	kb3	ktc3	kt1	kt2	kt3	kb2	kb3	ktc3
WR	0.0295	[psi]	161.45	15.98	8.41	3.89	1.94	4.32	159.71	15.93	8.39	3.88	1.94	4.31	1.08	0.30	0.19	0.21	0.14	0.11
	0.7493	*[ksi]*	1113.15	110.18	57.96	26.79	13.40	29.75	1101.16	109.85	57.85	26.74	13.38	29.72						
	0.0358	[psi]	288.55	28.56	15.02	6.95	3.47	7.71	285.40	28.47	14.99	6.93	3.47	7.70	1.09	0.30	0.19	0.21	0.14	0.11
	0.9093	*[ksi]*	1989.47	196.92	103.58	47.88	23.94	53.18	1967.74	196.33	103.38	47.78	23.91	53.12						
	0.0474	[psi]	669.74	66.29	34.87	16.12	8.06	17.90	662.19	66.09	34.80	16.09	8.05	17.88	1.13	0.31	0.20	0.21	0.14	0.12
	1.2040	*[ksi]*	4617.68	457.06	240.43	111.14	55.57	123.43	4565.66	455.64	239.94	110.91	55.49	123.28						
	0.0598	[psi]	1344.85	133.11	70.02	32.37	16.18	35.95	1329.06	132.68	69.87	32.30	16.16	35.90	1.17	0.32	0.21	0.22	0.15	0.12
	1.5189	*[ksi]*	9272.40	917.78	482.78	223.18	111.59	247.84	9163.55	914.82	481.75	222.69	111.42	247.53						
IR	0.0295	[psi]	99.12	16.36	8.92	1.22	0.61	4.67	98.50	16.32	8.90	1.22	0.61	4.66	0.62	0.23	0.15	0.15	0.10	0.07
	0.7493	*[ksi]*	683.41	112.79	61.47	8.44	4.22	32.18	679.17	112.53	61.38	8.43	4.22	32.16						
	0.0358	[psi]	177.15	29.24	15.93	2.19	1.09	8.34	176.04	29.17	15.91	2.19	1.09	8.34	0.63	0.23	0.15	0.15	0.10	0.07
	0.9093	*[ksi]*	1221.42	201.59	109.86	15.09	7.54	57.52	1213.72	201.12	109.69	15.07	7.54	57.48						
	0.0474	[psi]	411.18	67.86	36.98	5.08	2.54	19.36	408.50	67.70	36.92	5.07	2.54	19.35	0.65	0.24	0.16	0.16	0.11	0.07
	1.2040	*[ksi]*	2834.98	467.90	254.99	35.02	17.51	133.50	2816.50	466.76	254.58	34.97	17.49	133.40						
	0.0598	[psi]	825.66	136.27	74.26	10.20	5.10	38.88	820.03	135.92	74.14	10.18	5.09	38.85	0.68	0.26	0.17	0.16	0.11	0.08
	1.5189	*[ksi]*	5692.70	939.56	512.03	70.33	35.16	268.07	5653.89	937.15	511.15	70.22	35.13	267.86						
NR	0.0295	[psi]	64.88	14.20	7.97	0.66	0.33	4.25	65.75	14.27	8.00	0.66	0.33	4.25	1.34	0.55	0.36	0.34	0.22	0.14
	0.7493	*[ksi]*	447.34	97.87	54.95	4.52	2.26	29.27	453.34	98.41	55.14	4.53	2.26	29.31						
	0.0358	[psi]	115.96	25.37	14.24	1.17	0.59	7.59	117.51	25.51	14.29	1.18	0.59	7.60	1.34	0.55	0.36	0.34	0.22	0.14
	0.9093	*[ksi]*	799.51	174.92	98.20	8.08	4.04	52.31	810.18	175.88	98.55	8.10	4.05	52.39						
	0.0474	[psi]	269.15	58.89	33.06	2.72	1.36	17.61	272.70	59.21	33.17	2.73	1.36	17.63	1.32	0.54	0.35	0.33	0.22	0.13
	1.2040	*[ksi]*	1855.70	406.00	227.93	18.75	9.37	121.42	1880.21	408.21	228.73	18.81	9.39	121.59						
	0.0598	[psi]	540.45	118.24	66.38	5.46	2.73	35.36	547.48	118.87	66.61	5.48	2.74	35.41	1.30	0.53	0.34	0.33	0.22	0.13
	1.5189	*[ksi]*	3726.28	815.26	457.70	37.64	18.82	243.82	3774.76	819.59	459.24	37.77	18.86	244.13						
DR	0.0295	[psi]	19.13	2.59	1.39	0.43	0.21	0.72	19.29	2.60	1.39	0.43	0.21	0.72	0.84	0.27	0.17	0.19	0.12	0.09
	0.7493	*[ksi]*	131.92	17.87	9.58	2.94	1.47	4.97	133.03	17.92	9.60	2.94	1.47	4.98						
	0.0358	[psi]	34.20	4.63	2.48	0.76	0.38	1.29	34.48	4.64	2.49	0.76	0.38	1.29	0.83	0.27	0.17	0.19	0.12	0.08
	0.9093	*[ksi]*	235.78	31.93	17.13	5.25	2.63	8.89	237.74	32.02	17.15	5.26	2.63	8.89						
	0.0474	[psi]	79.37	10.75	5.77	1.77	0.88	2.99	80.03	10.78	5.77	1.77	0.88	2.99	0.83	0.27	0.17	0.19	0.12	0.08
	1.2040	*[ksi]*	547.25	74.11	39.75	12.19	6.09	20.62	551.77	74.31	39.82	12.21	6.10	20.64						
	0.0598	[psi]	159.38	21.58	11.58	3.55	1.77	6.01	160.68	21.64	11.60	3.56	1.78	6.01	0.82	0.27	0.17	0.18	0.12	0.08
	1.5189	*[ksi]*	1098.89	148.82	79.82	24.47	12.24	41.41	1107.85	149.22	79.95	24.52	12.25	41.45						